Supplementary Information

Priyanka N. deSouza[1,2,*], Phoebe Atsieno Oriama[3], Peter P Pedersen[4,5], Sebastian Horstmann[4,5], Lorena Gordillo-Dagallier[4,5], Charles N. Christensen[4,5], Christoph O. Franck[4,5], Richard Ayah[3], Ralph A. Kahn[6], Jacqueline M. Klopp[7], Kyle P. Messier[8], Patrick L. Kinney[9]

[1]: Department of Urban Studies and Planning, MIT, Cambridge MA 02139, USA

[2]: World Health Organization, Geneva 1202, Switzerland

[3]: University of Nairobi MakerSpace, Nairobi, Kenya

[4]: open-seneca, Cambridge CB3 0AS, United Kingdom

[5]: Department of Chemical Engineering and Biotechnology, University of Cambridge, Philippa Fawcett Drive, Cambridge CB3 0AS, United Kingdom

[6]: Climate and Radiation Laboratory, Earth Science Division, NASA Goddard Space Flight Center, Greenbelt, MD, USA

[7]:Center for Sustainable Urban Development, Earth Institute, Columbia University 475 Riverside Dr. Suite 520, New York NY 10115, USA

[8]: National Institute of Environmental Health Sciences, Division of the National Toxicology Program, USA

[9]: Boston University School of Public Health, Boston, MA, USA

*: Corresponding author

S1: Time of day of mobile monitoring

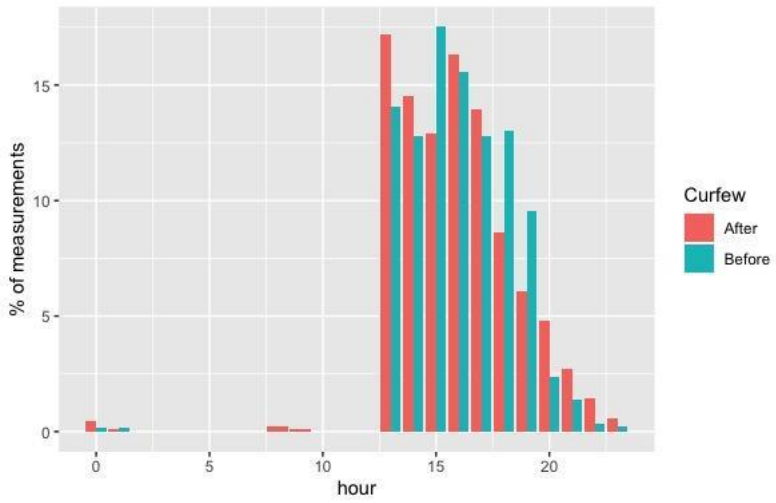

Figure S1: *Percentage of measurements made before and after the curfew for different hours of the day*

S2 Methods

S2.1 Mobile Monitoring Platform

In order to evaluate if self-emissions from the motorbikes affected the measurements, we evaluated the correlation between $PM_{2.5}$ concentrations and the calculated velocity (distance between measurements/time): -0.008, as well as with calculated acceleration of the vehicles (velocity between measurements/time) (0.004). The low correlations likely indicates that the self-emissions did not significantly affect our results. Other than self-emissions, there are other factors that can affect the performance of low-cost sensors in a mobile setting, such as wind speed, vibrations etc. Limited research has evaluated how these parameters impact the measurements from a specific low-cost sensor: the PurpleAir finds that the fidelity of the measurements decreases with increasing air flow velocities (Mui et al., 2021). There is a need to extend this important line of research to other low-cost sensors.

S2.2 SPS 30

The SPS 30 uses a proprietary algorithm to estimate the number concentration of particles in size bins ranging from 0.3-10 μm diameter, based on measurements of the amount of red laser

light scattered by the particles. A fan generates the sample flow. As the sensor is relatively new (introduced into the market in late 2018), no other field tests as of August 2020 have been published using this sensor as far as the authors are aware, though open-seneca is currently testing this sensor in other cities in Europe, South America and Asia.

Laboratory tests conducted by the South Coast Air Quality Management District in California USA also found low cross variability between sensors in their tests (http://www.aqmd.gov/docs/default-source/aq-spec/field-evaluations/sensirion-sps30-evaluation-kit---field-evaluation.pdf, Last accessed Aug 1, 2020). These tests also demonstrated that the PM_1 and $PM_{2.5}$ measurements exhibited good agreement with that of a reference instrument, but the PM_{10} values did not, which is consistent with recent research that found the sensor was most sensitive to particles between 0.3 and 1.3 µm. Therefore, we restrict our focus to $PM_{2.5}$ in this study. As we are interested in spatial patterns of $PM_{2.5}$, our experiment allows us to compare the signal from our devices over space.

S2.3 Background Correction

We assessed the background aerosol contribution using two different methods. The first method assigns the lowest 10^{th} percentile of $PM_{2.5}$ concentrations for a given sampling hour as the fixed background value for that period.

The second method uses a time-series, spline-of-minimums approach to estimate the background $PM_{2.5}$. It involves (a) applying a rolling 30-second mean to smooth the measurements, (b) dividing the time series into discrete 10-minute segments and locating the minimum concentration in each segment, and (c) fitting a smooth, thin-plate regression spline through the minimum concentrations. We include all observations made from the eight Sensirion SPS 30 sensors for a given day in this methodology, consistent with our assumption that the background is temporally varying but spatially uniform.

We compared each of the two proposed methods to choose a background pollution value and found that they produced similar background-corrected $PM_{2.5}$ values. The median differences in the background-corrected $PM_{2.5c}$ values using the different methods was ~ 4.4% (mean difference = -41%). The median differences between the $PM_{2.5c}$ values and the raw $PM_{2.5}$ measurements were also ~0% for both Methods (mean= 3.1% for Method 1 and -18.3% for Method 2). Note that the mean values are higher because the different background corrections produce different values

for large spikes in $PM_{2.5}$ measurements. There are few such spikes in the data. Given the small differences in median $PM_{2.5c}$ values from the two methods, we chose the splines-of-minimum approach to obtain background concentrations. This is supported by previous research that found this approach to be an effective way to account for background concentrations for a range of pollutants over a variety of meteorological conditions and sampling routes (Brantley et al., 2014).

S3 Covariates for Land-Use Regression

The following section delineates the socioeconomic, land-use and transportation-related independent variables used in the random forest model.

S3.1 Poverty Index

2008 estimates of proportion of people per 1 km x 1km grid cell living in poverty, as defined by the Multidimensional Poverty Index (MPI) (http://www.ophi.org.uk/policy/multidimensional-poverty-index/, last accessed June 29, 2020), were obtained from WorldPop (**Figure S2** in Supplementary Information). Briefly, Bayesian model-based geostatistics were used to derive these estimates, in combination with high resolution gridded spatial covariates applied to GPS-located household survey data on poverty from the Kenyan Demographic Health Survey. This index encompasses the various deprivations experienced by people in their daily lives by incorporating indicators that fall in three dimensions: Education (Years of schooling, School attendance), Health (Child mortality, Nutrition) and Standard of Living (Cooking Fuel, Sanitation, Water, Electricity, Floor, Asset Ownership). The Alkire-Foster (AF) method was used to compute the MPI by combining these indicators.

As displayed in **Figure S2**, the eastern part of the city is poorer than western part. Scholars have shown that the deeply rooted class-based segregation patterns in Nairobi align closely with racial segregation patterns created during the colonial period. Therefore, although poverty may have intensified in certain locations in later years, the overall pattern in 2020 is likely to be the same as in 2008. Note that the poverty index is coarse and doesn't appear to capture poorer neighborhoods closer to the city center which are densely populated (**Figure S2).**

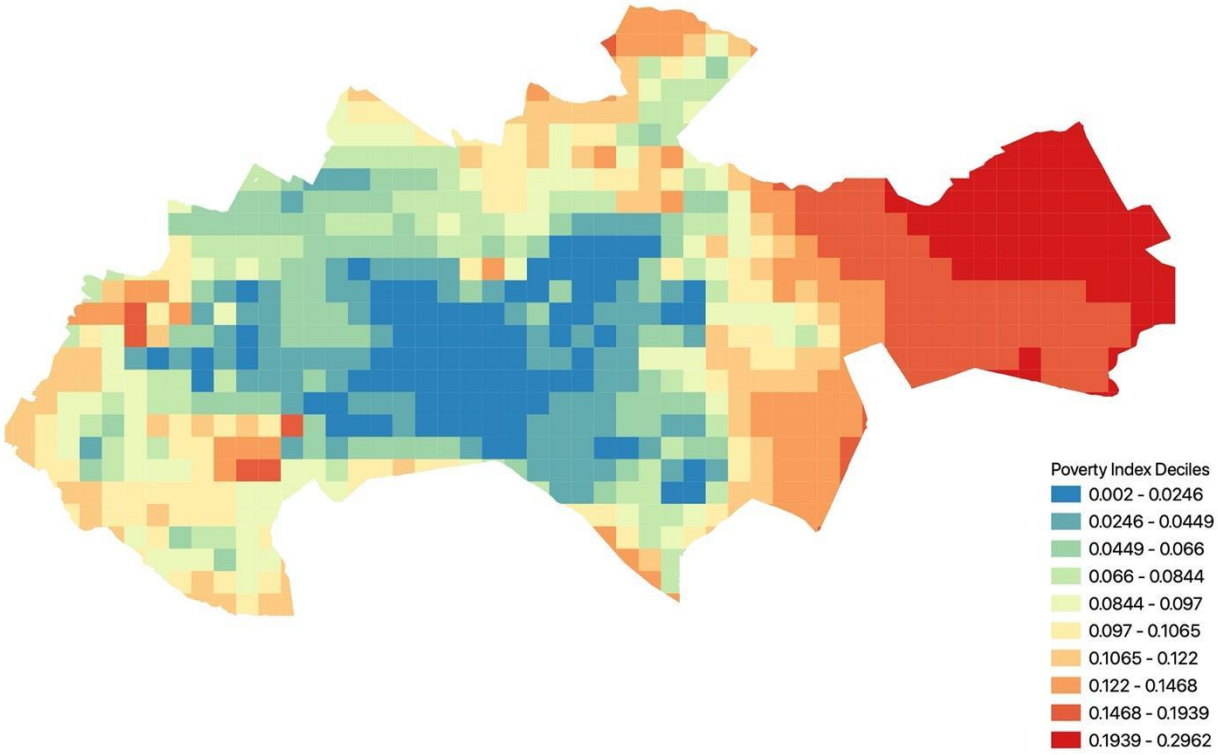

***Figure S2**: Poverty index classified into deciles for Nairobi and its immediate environs*

S3.2 Population Density

2015 population estimates for each 100 m x 100 m grid cell in Nairobi (**Figure S3** in Supplementary Information) were obtained from WorldPop (https://www.worldpop.org/geodata/summary?id=83, Last Accessed June 12, 2020).

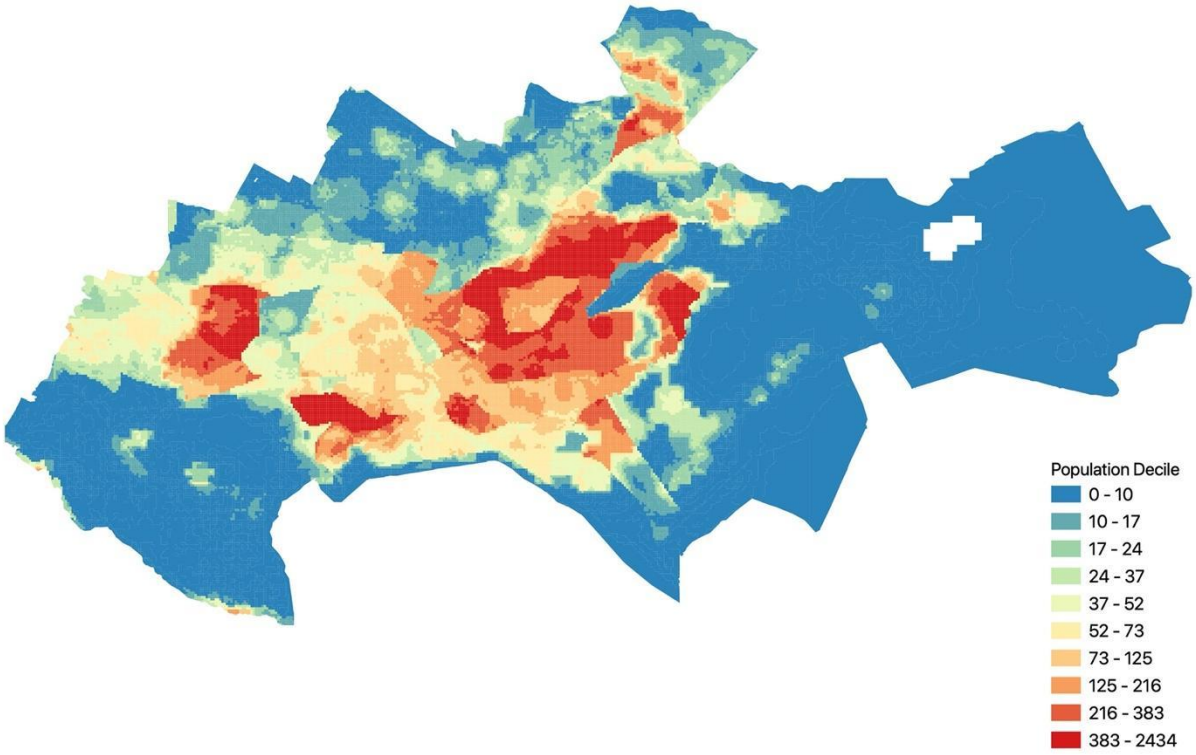

Figure S3*: Population density classified into deciles for Nairobi and its immediate environs*

S3.3 Land-Use

Columbia University digitized plat maps of Nairobi to produce a land use map for the city in 2005 (http://csud.ei.columbia.edu/projects/nairobi-regional-project/nairobi-gis-maps/ , Last accessed July 11, 2020). This map was updated and validated for the year 2010 in partnership with the University of Nairobi (**Figure S4** in Supplementary Information).

Although, more recent pdf versions of land use in Nairobi are available and reproduced in the Nairobi Integrated Urban Development Master Plan produced by the Japanese International Cooperation Agency (JICA), the data from the newer map has not been made publicly available.

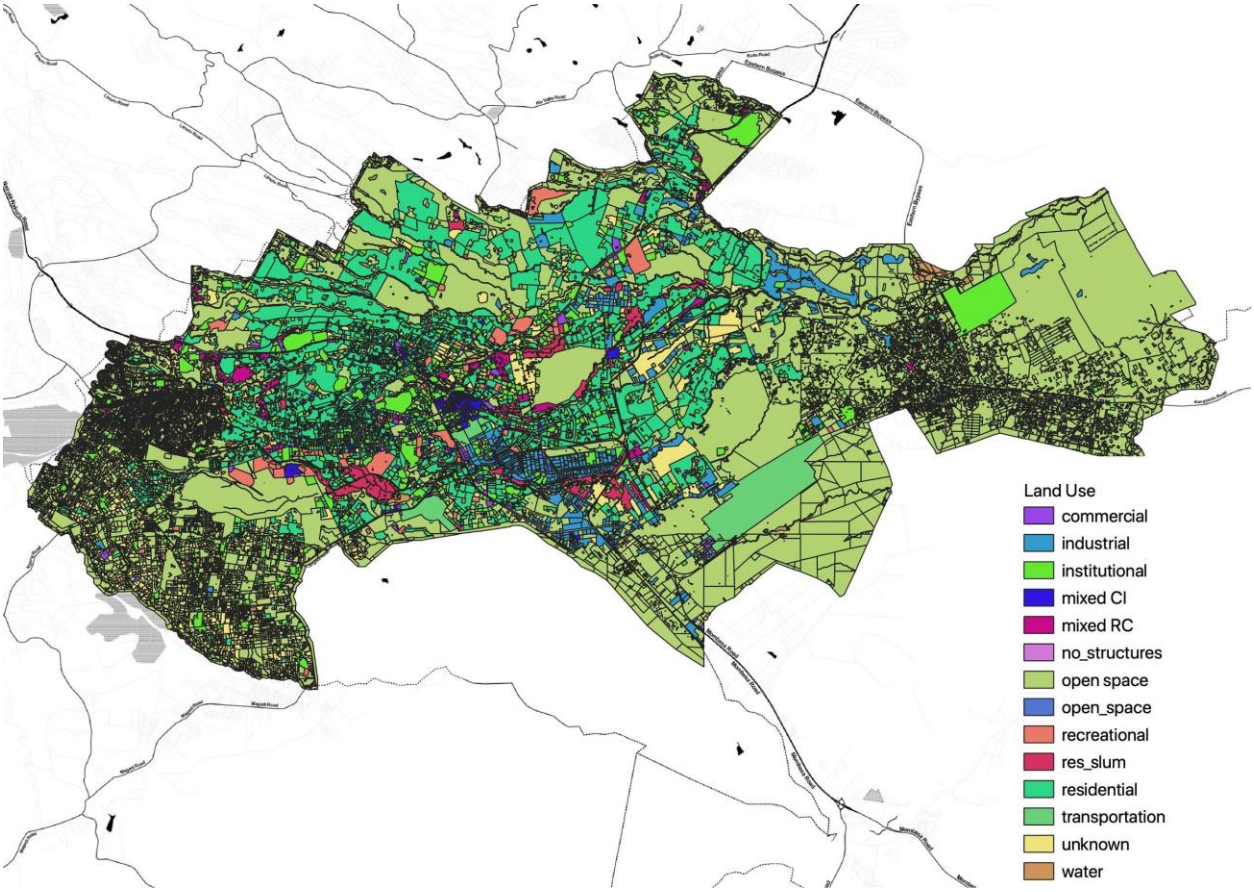

Figure S4: *Land-use in Nairobi in 2010*

S3.4 Transportation-related sources

A surrogate for traffic: average travel friction (min-m^{-1}), or travel time was obtained from the University of Oxford Malaria Atlas Project (https://malariaatlas.org/research-project/accessibility-to-cities/) global travel friction dataset at a 1 km x 1 km scale (Pfeffer et al., 2018).

We also downloaded the Nairobi roads shapefile, which classified roads into 1) Bound Surface, 2) Cutline, 3) Dry Weather Roads, 4) Loose Surface, 5) Main Track (Motorable), from (http://www.virtualkenya.org/).

We downloaded matatu (the main form of public transport) stops from the Digital Matatus project that were updated as of 2019 (http://www.digitalmatatus.com/map.html). We also downloaded the number of matatu trips associated with each stop. This serves as a proxy of how busy each matatu stop was.

Unfortunately, no information about the use of biomass for household energy purposes or industrial sources were available for Nairobi.

S3.5 Neighborhoods

We downloaded the administrative boundaries of Nairobi from Diva-GIS (https://www.diva-gis.org/gdata) (**Figure S5**).

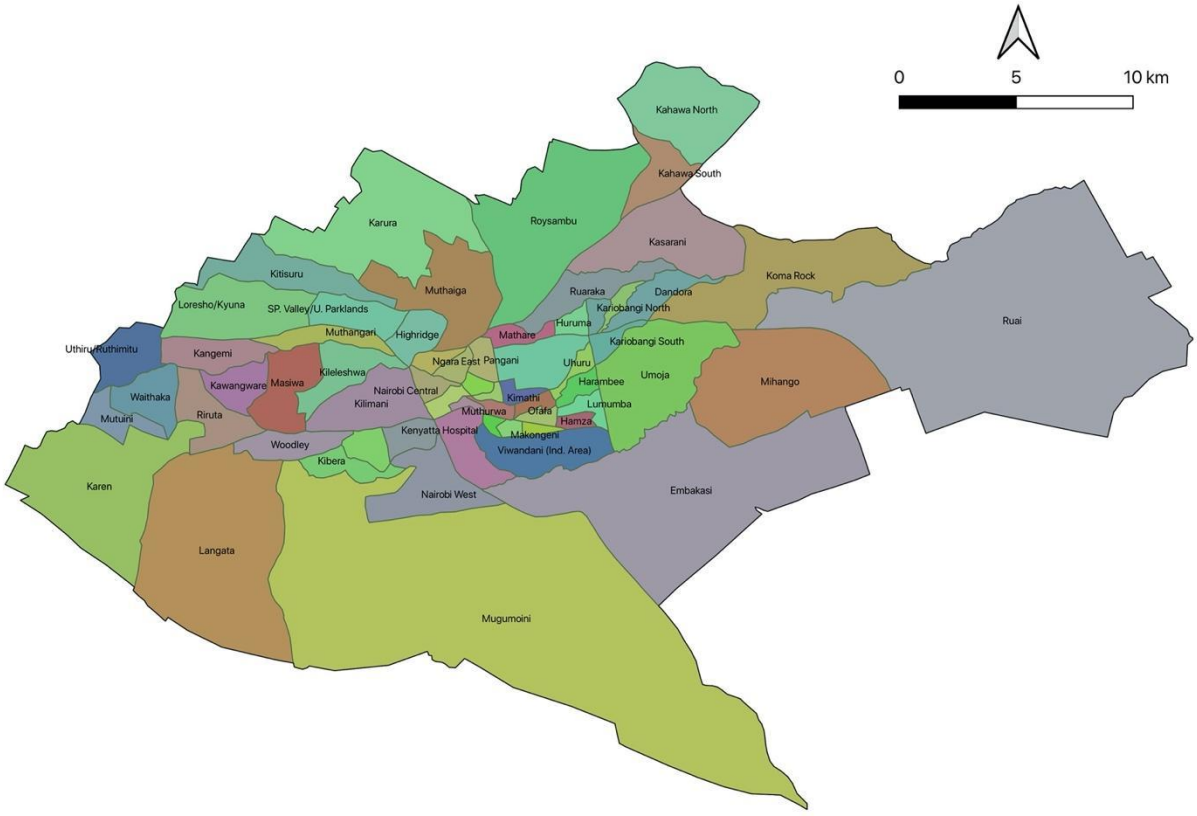

Figure S5: *Nairobi neighborhoods*

S4 Random Forest Cross Validation

Our 10-fold cross-validation (CV) exercise occurred in the following manner: The model fitting dataset was randomly split into 10 groups, with each group containing about 10% of the grid cells. In each cross-validation iteration, we select nine groups of the grid cells. All of the data

from these grid cells are used to fit the model and make predictions of the remaining group. We repeated this process 10 times, until every group was predicted.

The CV process was used to tune two major RF hyperparameters: the number of decision trees (n_{tree}) and the number of predictors randomly tried at each split (m_{try}). Briefly, the optimal m_{try} was determined by optimizing the "pseudo R^2": the fraction of variance of the $PM_{2.5c}$ measurements explained by the "out of bag" (OOB) predictions. An OOB prediction is based only on trees in the random-forest ensemble that were not trained using the $PM_{2.5c}$ observations being predicted. Each m_{try} value was used to train 10 random-forests. The average pseudo R^2 was used to select the best m_{try} value. A Moran I test on the residuals of the RF model was conducted to confirm that there was no spatial autocorrelation that we needed to account for.

S5 Universal Kriging

Kriging is a geostatistical interpolation technique that works on the assumption that the spatial variation in the feature ($PM_{2.5}$) is homogeneous over the domain and depends only on the distance between sites. Spatial dependence is the property of observations over space to exhibit functional similarity as a result of proximity (Jerrett et al., 2005). Kriging models are considered optimal interpolators as they provide the best linear unbiased estimate of the value of the variable at any point in the coverage (Burrough and McDonnell, 1998). The universal kriging procedure, unlike ordinary kriging, incorporates a drift function to account for a structural component in the spatial variation. A linear drift function was selected in this study because this method resulted in lower kriging variances in $PM_{2.5c}$ estimates than did a quadratic drift function. We use the natural logarithm to transform $PM_{2.5c}$ concentrations for this interpolation technique to obtain a more uniform distribution.

In order to provide a function that describes the spatial dependence of the $PM_{2.5c}$ concentrations, we used the package '*automap*' in R to automatically fit a variogram to the data. This package iterates over various variogram models to pick the model that has the lowest residual sum of squares. We also attempted to interpolate $PM_{2.5c}$ concentrations using kriging with an external drift that allows the mean $PM_{2.5c}$ values over space to depend on external spatial variables, in addition to the internal drift with the spatial coordinates. However, including

the covariates described in **Section S2** in the **SI**, namely the MPI, population density, land-use type, transportation-related covariates such as the density of different types of roadways, travel friction, matatu stops and matatu trips, and area of different overlapping neighbourhoods in a linear manner did not improve the model. We therefore did not include an external drift in the final model.

As in the case of the RF, we also conducted a 10-fold cross validation (CV) exercise. We report the RMSE and R^2 of the best model determined from the CV exercise.

S6 Results

S6.1 Mobile monitoring estimates

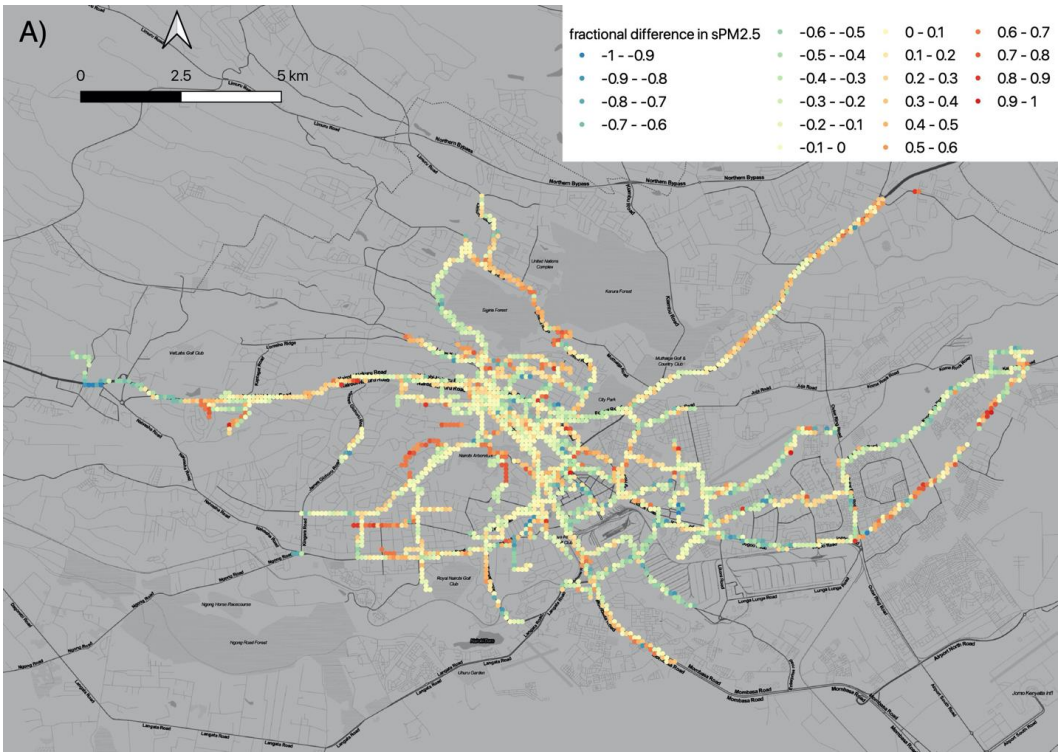

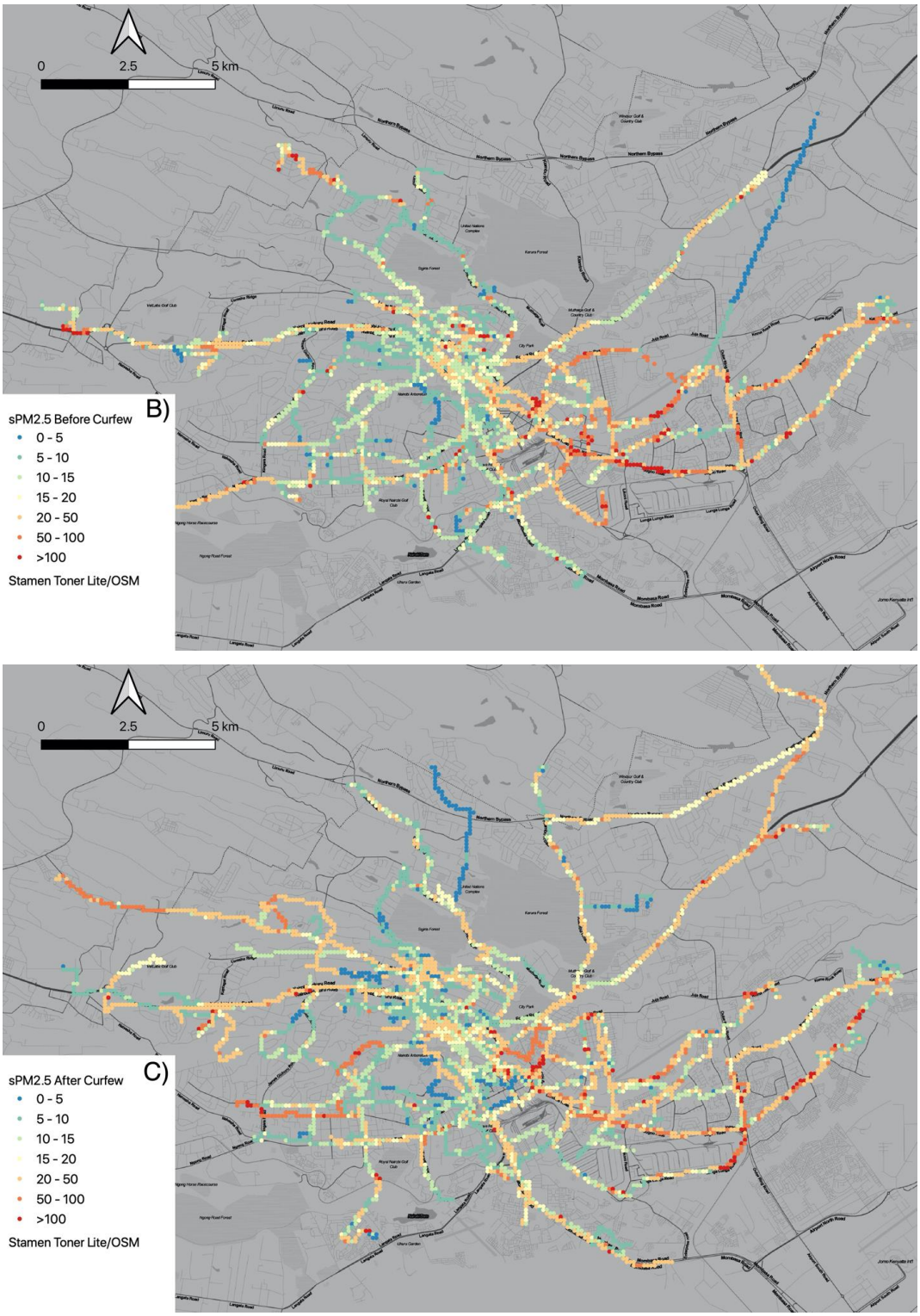

Figure S6: *a) The fractional change* $((PM_{2.5c,after} - PM_{2.5c,before})/(PM_{2.5c,before} + PM_{2.5c,before})$ *in* $PM_{2.5c}$ *after the curfew was imposed, from March 25, 2020 - May 5, 2020, compared to levels for each*

100 m grid cell from March 13, 2020 - March 25, 2020, Median $PM_{2.5c}$ values for each 100 m grid cell in Nairobi b) before and c) after the curfew had started in units of $\mu g/m^3$

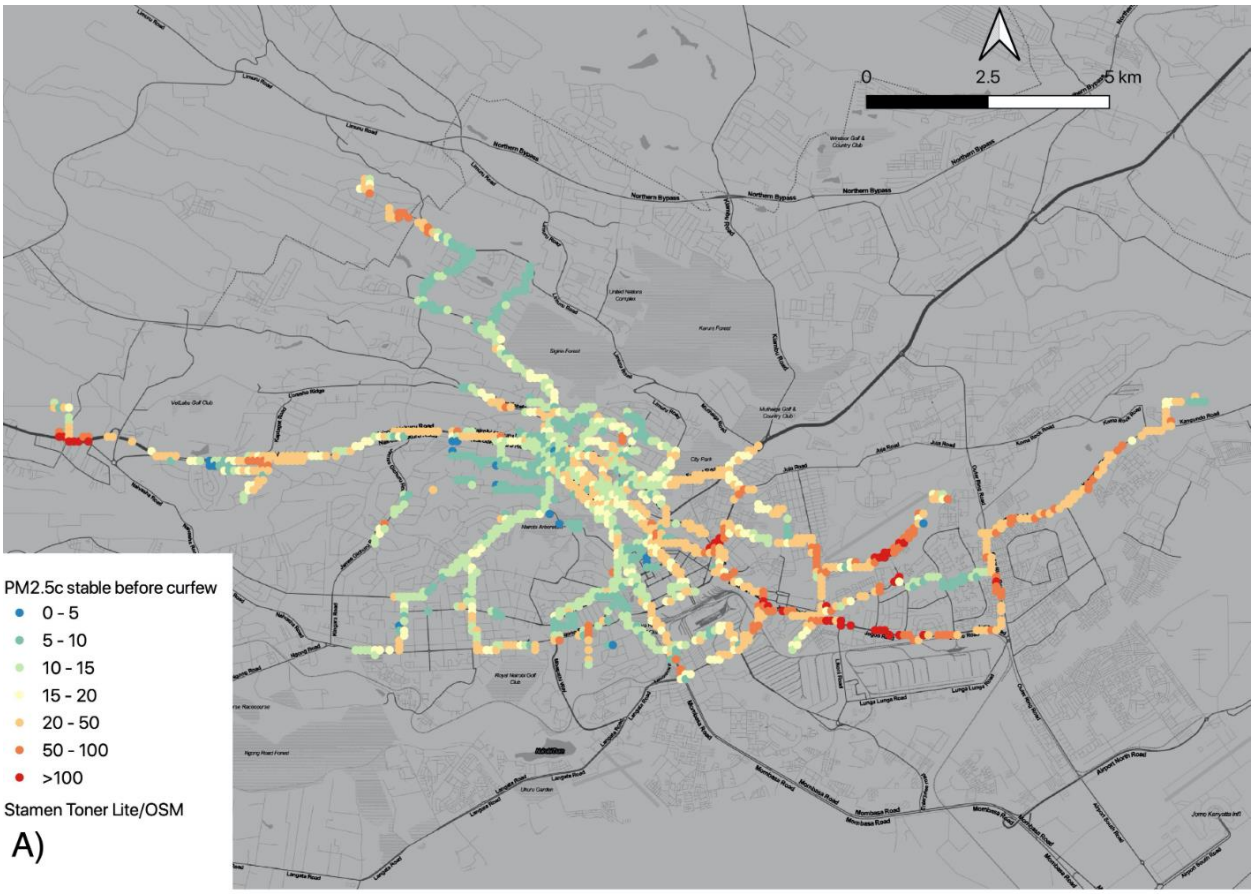
0
2.5
5 km
PM2.5c stable before curfew
0 - 5
5 - 10
10 - 15
15 - 20
20 - 50
50 - 100
>100
Stamen Toner Lite/OSM

A)

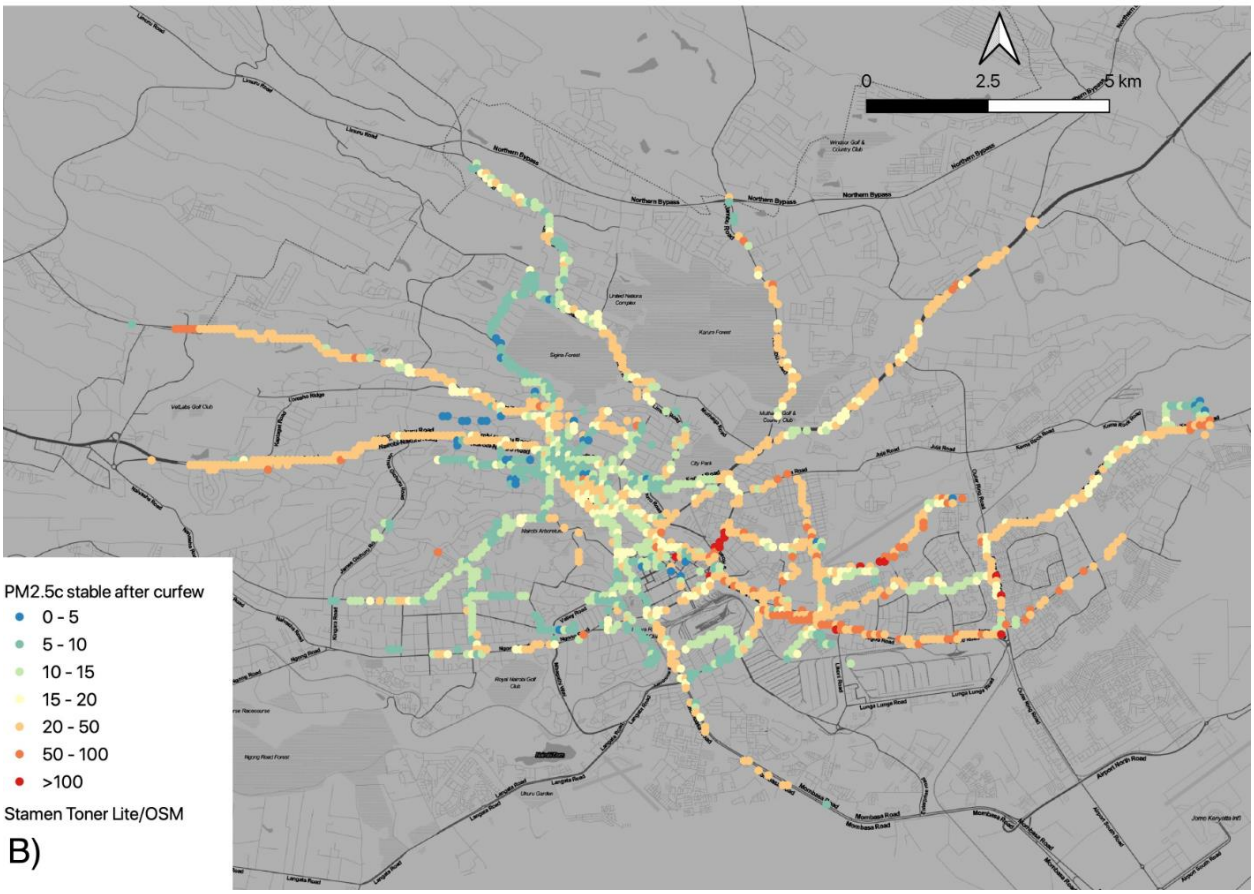
0
2.5
5 km
PM2.5c stable after curfew
0 - 5
5 - 10
10 - 15
15 - 20
20 - 50
50 - 100
>100
Stamen Toner Lite/OSM

B)

Figure S7: *$PM_{2.5c}$ values for grid cells for which the median was stable (normalized error in median < 20% and the number of days over which the grid cell was sampled > 1) b) before and c) after the curfew had started in units of $\mu g/m^3$*

S6.2 : Random forest results run using stable $PM_{2.5c}$ values only

Mean $PM_{2.5}$ concentration before the COVID-19 curfew predicted using this mode was 34.0 $\mu g/m^3$ (Median: 34.0 $\mu g/m^3$). Mean concentration during the COVID-19 curfew was: 26.0 $\mu g/m^3$ (Median: 26.5 $\mu g/m^3$). A Wilcoxon rank sum test revealed a statistically significant decrease in $PM_{2.5}$ concentrations in Nairobi overall during the COVID-19 crisis for the time-period of this study.

The top-five variables with the highest predictive power during before the curfew were: 1) Longitude, 2) The length of railway lines in the 500 m buffer around each grid cell, 3) Area of the Lumumba neighborhood in the 100 m buffer of each grid cell, 4) Area of unknown land in the 500 m buffer around each grid cell, 5) Area of the Loresho/Kyuna neighborhood in the 100 mbuffer of each grid cell.

The top-five variables with the highest predictive power during the curfew were: 1) Longitude, 2) The area of the neighborhood Pangani in the 100 m buffer around each grid cell, 3) The length of dry weather roads in the 500 m buffer around each grid cell, 4) The length of all roads in the 500 m around each grid cell, 5) The area of residential land in the 500 m of each grid cell.

The 10-fold cross-validation approach for the RF model using data before and during the COVID-19 curfew yielded RMSEs (MAEs) of 10 $\mu g/m^3$ (3 $\mu g/m^3$) and 7 $\mu g/m^3$ (4 $\mu g/m^3$), respectively. The R^2 value of the cross-validated models before and during the COVID-19 curfew were both 0.96.

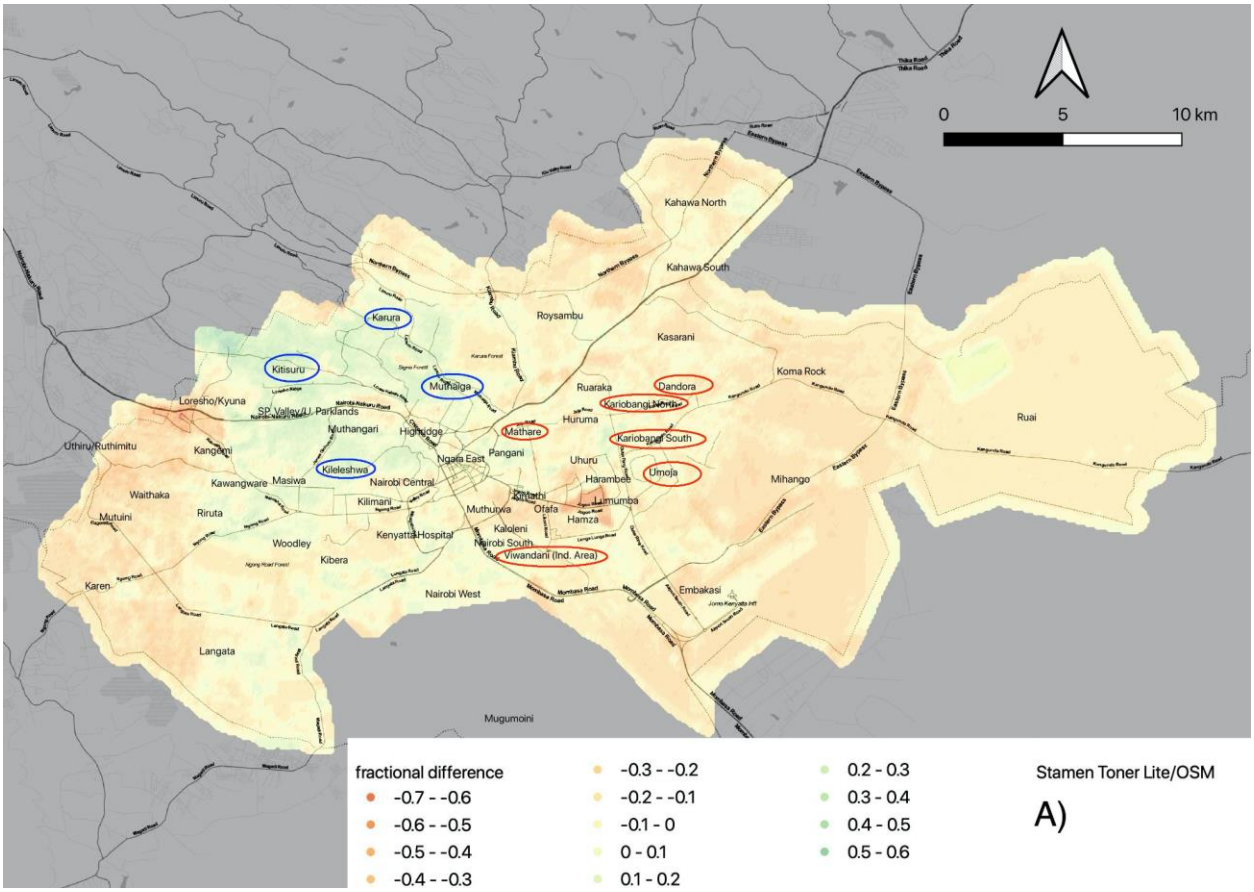
0
5
10 km
Kahawa North
Kahawa South
Karura
Roysambu
Kasarani
Kitisuru
Muthaiga
Ruaraka
Dandora
Koma Rock
Loresho/Kyuna
SP Valley/U. Parklands
Kariobangi North
Huruma
Ruai
Muthangari
Highridge
Mathare
Kariobangi South
Uthiru/Ruthimitu
Kangemi
Ngara East
Pangani
Uhuru
Umoja
Kileleshwa
Harambee
Mihango
Kawangware
Masiwa
Nairobi Central
Waithaka
Kilimani
Kirichi
Ofafa
Jamumbia
Mutuini
Riruta
Muthurwa
Hamza
Kenyatta Hospital
Kaloleni
Woodley
Nairobi South
Kibera
Viwandani (Ind. Area)
Karen
Nairobi West
Embakasi
Langata
Mugumoini
fractional difference
-0.7 - -0.6
-0.6 - -0.5
-0.5 - -0.4
-0.4 - -0.3
-0.3 - -0.2
-0.2 - -0.1
-0.1 - 0
0 - 0.1
0.1 - 0.2
0.2 - 0.3
0.3 - 0.4
0.4 - 0.5
0.5 - 0.6
Stamen Toner Lite/OSM
A)

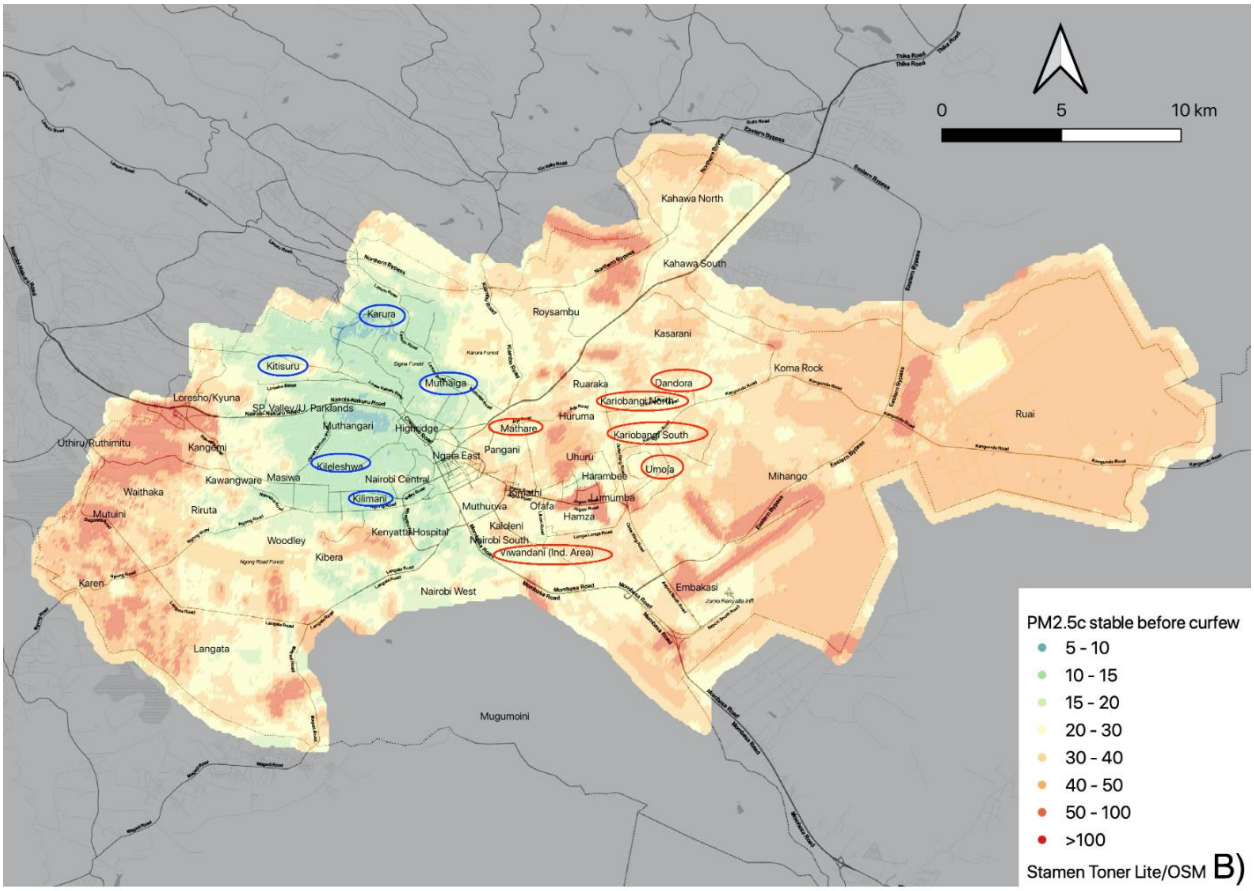
0
5
10 km
Kahawa North
Kahawa South
Karura
Roysambu
Kasarani
Kitisuru
Muthaiga
Ruaraka
Dandora
Koma Rock
Loresho/Kyuna
SP Valley/U. Parklands
Kariobangi North
Ruai
Muthangari
Highridge
Mathare
Huruma
Kariobangi South
Uthiru/Ruthimitu
Kangemi
Ngara East
Pangani
Uhuru
Kileleshwa
Harambee
Umoja
Mihango
Kawangware
Masiwa
Nairobi Central
Waithaka
Kilimani
Muthurwa
Ofafa
Limumba
Mutuini
Riruta
Hamza
Kenyatta Hospital
Kaloleni
Woodley
Nairobi South
Kibera
Viwandani (Ind. Area)
Karen
Nairobi West
Embakasi
Langata
Mugumoini
PM2.5c stable before curfew
5 - 10
10 - 15
15 - 20
20 - 30
30 - 40
40 - 50
50 - 100
>100
Stamen Toner Lite/OSM
B)

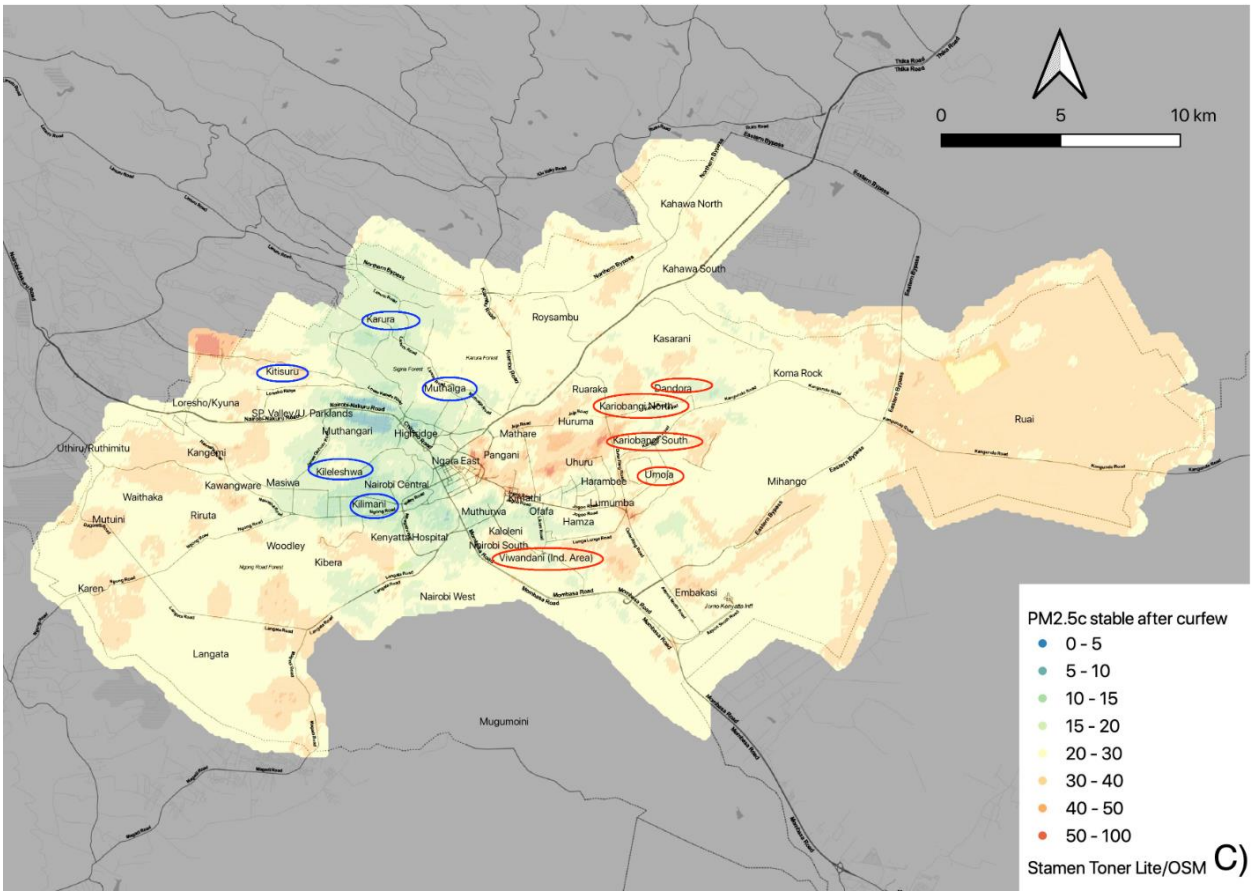
0
5
10 km
Kahawa North
Kahawa South
Karura
Roysambu
Kasarani
Kitisuru
Muthaiga
Ruaraka
Dandora
Koma Rock
Loresho/Kyuna
SP Valley/U. Parklands
Kariobangi North
Ruai
Muthangari
Highridge
Mathare
Huruma
Kariobangi South
Uthiru/Ruthimitu
Kangemi
Ngara East
Pangani
Uhuru
Kileleshwa
Harambee
Umoja
Mihango
Kawangware
Masiwa
Nairobi Central
Waithaka
Kilimani
Muthurwa
Ofafa
Limumba
Mutuini
Riruta
Hamza
Kenyatta Hospital
Kaloleni
Woodley
Nairobi South
Kibera
Viwandani (Ind. Area)
Karen
Nairobi West
Embakasi
Langata
Mugumoini
PM2.5c stable after curfew
0 - 5
5 - 10
10 - 15
15 - 20
20 - 30
30 - 40
40 - 50
50 - 100
Stamen Toner Lite/OSM
C)

Figure S8: *a) The fractional change* ($PM_{2.5cafter}$ - $PM_{2.5cbefore}$)/($PM_{2.5c,before}$ + $PM_{2.5c,before}$) *in predicted* $PM_{2.5c}$ *after the curfew was imposed, from March 25, 2020 - May 5, 2020, compared to predicted levels before. Estimated* $PM_{2.5c}$ *values for each 100 m grid cell in Nairobi b) before and c) after the curfew in units of* $\mu g/m^3$ *using RF models.* $PM_{2.5c}$ *concentrations were estimated via a random forest using grid cells with a stable* $PM_{2.5c}$ *only. The poorer neighborhoods in Nairobi are circled in red and the wealthier neighborhoods are circled in blue.*

S6.3 : Universal Kriging

Mean $PM_{2.5}$ concentration before the COVID-19 curfew interpolated using kriging was 17.2 $\mu g/m^3$ (Median: 14.8 $\mu g/m^3$). Mean concentration during the COVID-19 curfew was: 22.0 $\mu g/m^3$ (Median: 21.3 $\mu g/m^3$). A Wilcoxon rank sum test revealed a statistically significant increase in $PM_{2.5}$ concentrations in Nairobi overall during the COVID-19 crisis for the time-period of this study.

The R^2 from the Universal Kriging before the curfew was 0.66 and after was 0.64. The RMSEs (MAE) values were 28 $\mu g/m^3$ (11 $\mu g/m^3$) and 30 $\mu g/m^3$ (10 $\mu g/m^3$) before and during the curfew respectively. Mean predicted $PM_{2.5c}$ concentrations before the COVID-19 curfew was 17.2 $\mu g/m^3$ (Median: 14.8 $\mu g/m^3$). Mean predicted concentration during the COVID-19 curfew was a little higher: 21.6 $\mu g/m^3$ (Median: 21.3 $\mu g/m^3$). The lack of variation in the $PM_{2.5}$ surfaces derived from this approach in the outskirts of Nairobi (Ruai in the east and Karen in the west as displayed in **Figure S7**), indicate the uncertainty in predictions due to the lack of measurements in these neighbourhoods. However, in areas close to the city center where the majority of measurements had been made, we see the results from this approach agree well with that of the RF predictions displayed in the main analysis.

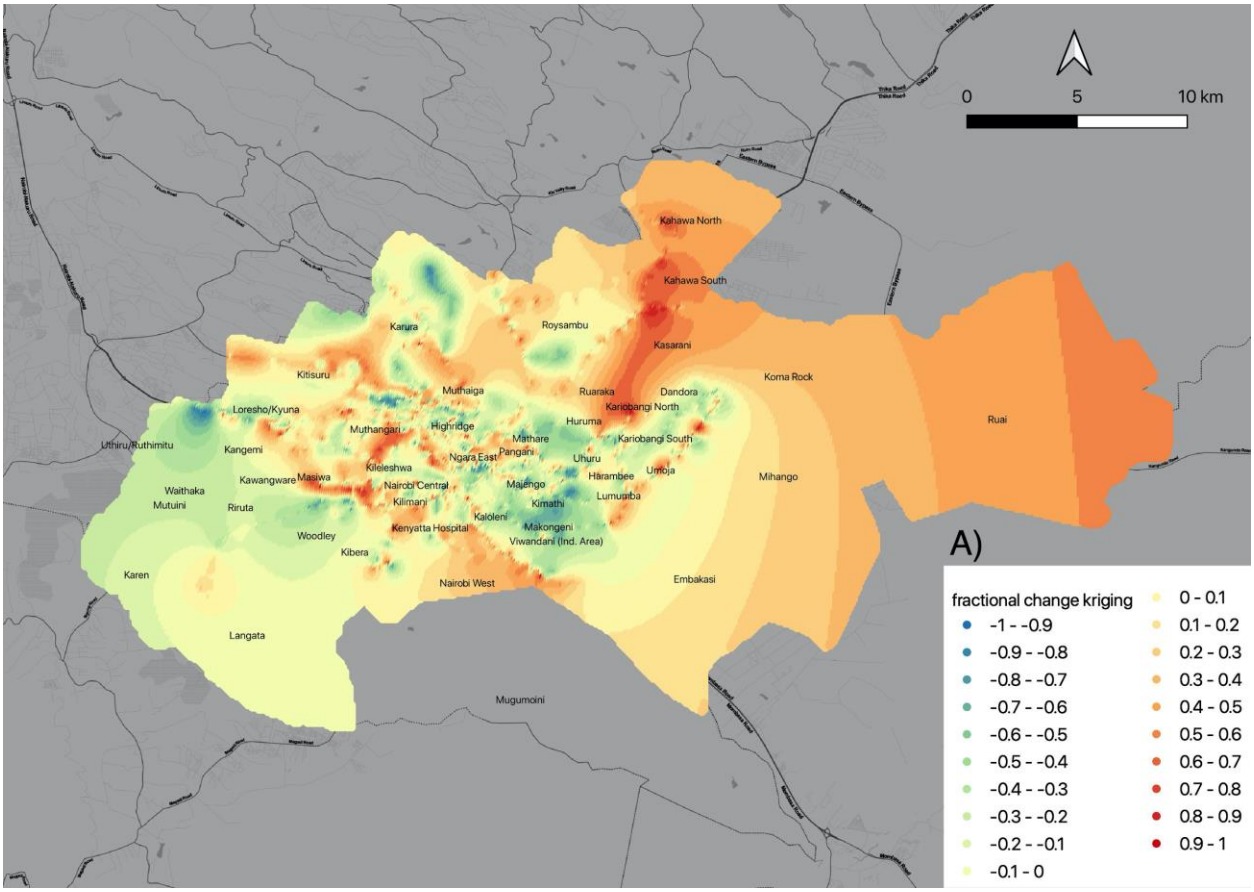
0
5
10 km
Kahawa North
Kahawa South
Karura
Roysambu
Kasarani
Kitisuru
Muthaiga
Ruaraka
Dandora
Koma Rock
Loresho/Kyuna
Kariobangi North
Ruai
Muthangari
Highridge
Huruma
Uthiru/Ruthimitu
Kangemi
Mathare
Kariobangi South
Ngara East
Pangani
Uhuru
Kileleshwa
Umoja
Kawangware
Masiwa
Nairobi Central
Harambee
Mihango
Waithaka
Majengo
Mutuini
Kilimani
Lumumba
Riruta
Kimathi
Kaloleni
Kenyatta Hospital
Makongeni
Woodley
Viwandani (Ind. Area)
Kibera
A)
Karen
Nairobi West
Embakasi
Langata
Mugumoini
fractional change kriging
-1 - -0.9
-0.9 - -0.8
-0.8 - -0.7
-0.7 - -0.6
-0.6 - -0.5
-0.5 - -0.4
-0.4 - -0.3
-0.3 - -0.2
-0.2 - -0.1
-0.1 - 0
0 - 0.1
0.1 - 0.2
0.2 - 0.3
0.3 - 0.4
0.4 - 0.5
0.5 - 0.6
0.6 - 0.7
0.7 - 0.8
0.8 - 0.9
0.9 - 1

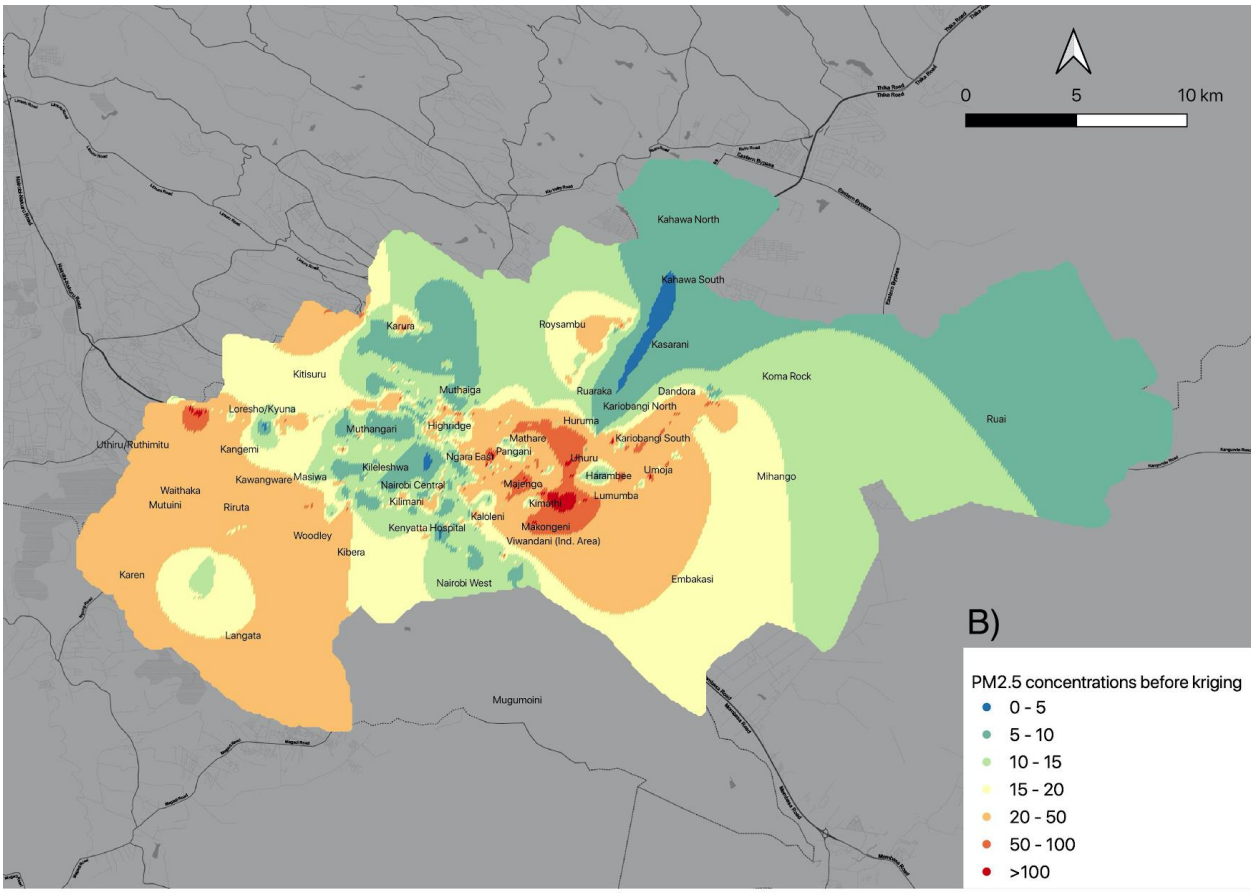
0
5
10 km
Kahawa North
Kahawa South
Karura
Roysambu
Kasarani
Kitisuru
Koma Rock
Muthaiga
Ruaraka
Dandora
Loresho/Kyuna
Kariobangi North
Ruai
Highridge
Huruma
Muthangari
Uthiru/Ruthimitu
Kangemi
Mathare
Kariobangi South
Ngara East
Pangani
Uhuru
Kileleshwa
Umoja
Kawangware
Masiwa
Harambee
Mihango
Nairobi Central
Majengo
Waithaka
Mutuini
Kilimani
Lumumba
Riruta
Kenyatta Hospital
Kaloleni
Kimathi
Woodley
Makongeni
Viwandani (Ind. Area)
Kibera
Karen
Nairobi West
Embakasi
Langata
Mugumoini
B)
PM2.5 concentrations before kriging
0 - 5
5 - 10
10 - 15
15 - 20
20 - 50
50 - 100
>100

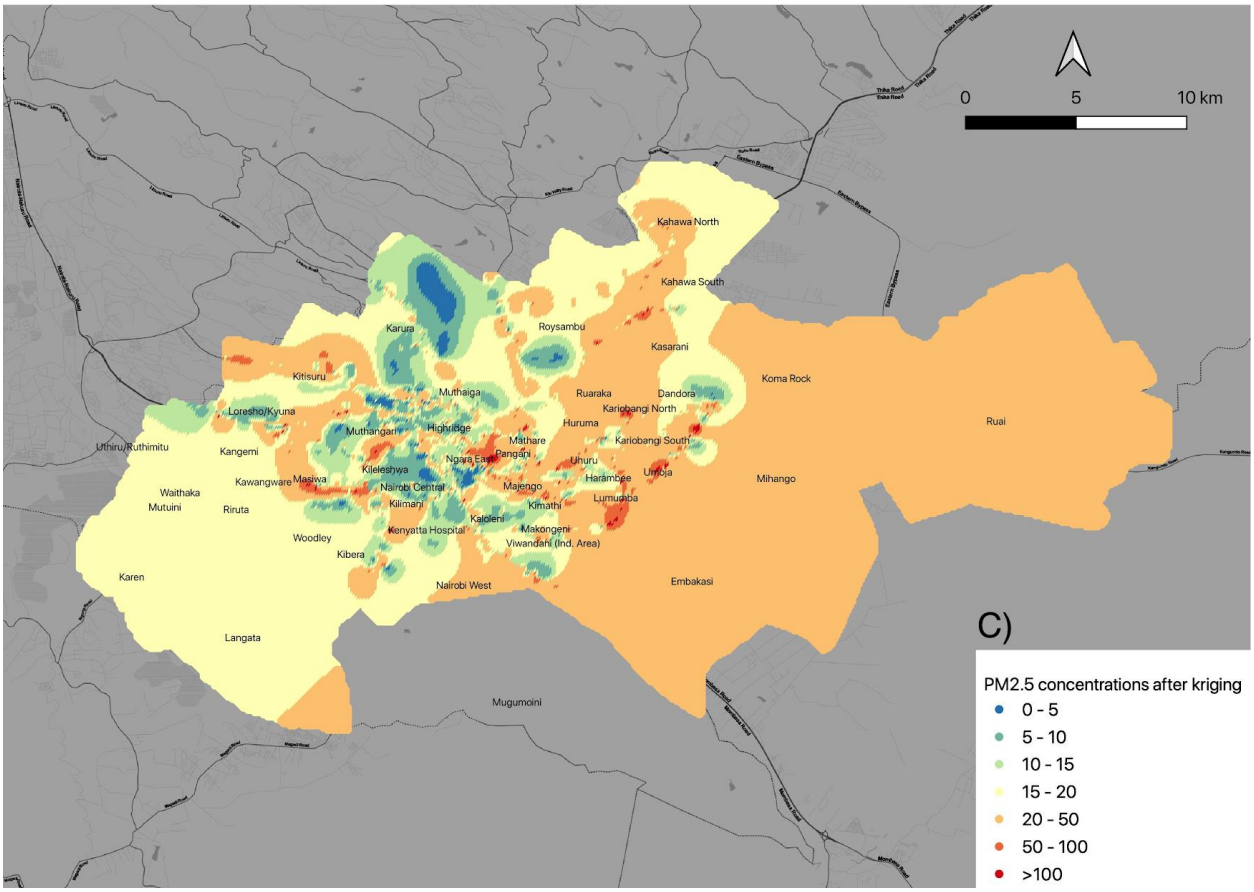
0
5
10 km
Kahawa North
Kahawa South
Karura
Roysambu
Kasarani
Kitisuru
Koma Rock
Muthaiga
Ruaraka
Dandora
Loresho/Kyuna
Kariobangi North
Ruai
Highridge
Huruma
Muthangari
Uthiru/Ruthimitu
Kangemi
Mathare
Kariobangi South
Ngara East
Pangani
Uhuru
Kileleshwa
Umoja
Kawangware
Masiwa
Harambee
Mihango
Nairobi Central
Majengo
Waithaka
Mutuini
Kilimani
Lumumba
Riruta
Kenyatta Hospital
Kaloleni
Kimathi
Woodley
Makongeni
Viwandani (Ind. Area)
Kibera
Karen
Nairobi West
Embakasi
Langata
Mugumoini
C)
PM2.5 concentrations after kriging
0 - 5
5 - 10
10 - 15
15 - 20
20 - 50
50 - 100
>100

Figure S9: *a) The fractional change* ($PM_{2.5c,after}$ - $PM_{2.5c,before}$)/($PM_{2.5c,before}$ + $PM_{2.5c,before}$) *in interpolated* $PM_{2.5c}$ *via universal kriging after the curfew was imposed, from March 25, 2020 - May 5, 2020, compared to interpolated levels before, Median* $PM_{2.5c}$ *values for each 100 m grid cell in Nairobi b) before and c) after the curfew in units of* mg/m^3.

References

Brantley, H., Hagler, G., Kimbrough, E., Williams, R., Mukerjee, S., Neas, L., 2014. Mobile air monitoring data-processing strategies and effects on spatial air pollution trends. Atmospheric Meas. Tech. 7.

Burrough, P.A., McDonnell, R., McDonnell, R.A. and Lloyd, C.D., 2015. Principles of geographical information systems. Oxford university press.

Jerrett, M., Burnett, R.T., Ma, R., Pope III, C.A., Krewski, D., Newbold, K.B., Thurston, G., Shi, Y., Finkelstein, N., Calle, E.E. and Thun, M.J., 2005. Spatial analysis of air pollution and mortality in Los Angeles. *Epidemiology*, pp.727-736.

Mui, W., Der Boghossian, B., Collier-Oxandale, A., Boddeker, S., Low, J., Papapostolou, V. and Polidori, A., Development of a Performance Evaluation Protocol for Air Sensors Deployed on a Google Street View Car. *Environmental Science & Technology*.

Pfeffer, D.A., Lucas, T.C., May, D., Harris, J., Rozier, J., Twohig, K.A., Dalrymple, U., Guerra, C.A., Moyes, C.L., Thorn, M. and Nguyen, M., 2018. malariaAtlas: an R interface to global malariometric data hosted by the Malaria Atlas Project. *Malaria journal*, *17*(1), pp.1-10.